



# Experimental Investigation of Spray-Deposited Fe-Doped ZnO Nanoparticle Thin Films: Structural, Microstructural, and Optical Properties

C. S. Prajapati, Ajay Kushwaha, and P. P. Sahay

(Submitted May 4, 2013; in revised form July 22, 2013)

Structural, microstructural, and optical properties of the undoped and Fe-doped zinc oxide (ZnO) thin films grown by spray pyrolysis technique using zinc nitrate as a host precursor have been reported here. X-ray diffraction spectra confirm that all the films have stable wurtzite structure and the effects of Fe dopants on the diffraction patterns have been found to be in agreement with the Vegard's law. Scanning electron microscopy results show good uniformity and dense surface having spherical-shaped grains. Energy dispersive x-ray analyses with elemental mapping of the Fe-doped films show that the Fe dopants are incorporated homogeneously into the ZnO film matrix. The x-ray photoelectron spectroscopy spectra confirm the presence of 3+ oxidation state of Fe in the doped films. Atomic force microscopy analyses clearly show that the average surface roughness and the grain size decrease with the addition of Fe dopants. Optical studies reveal that the optical band gap value decreases on Fe doping. The 1 at.% Fe-doped film shows normal dispersion for the wavelength range 450–700 nm. The PL spectra of the films show a strong ultraviolet emission centered at ~388 nm in the case of 1 at.% Fe-doped film. A slow photo current response in the films has been observed in the transient photoconductivity measurement.

**Keywords** Fe-doping, optical properties, surface morphology, ZnO nanoparticle thin films

## 1. Introduction

Zinc oxide (ZnO), a wide band gap (3.36 eV at 300 K) compound semiconductor, has a stable wurtzite structure and high exciton binding energy of 60 meV (Ref 1). It has drawn the attention of many researchers because of its unique properties such as high thermal stability, non-toxicity in nature, high transparency in visible region, good phosphor material, etc. Because of its multifunctional properties (semiconducting, magnetic, piezoelectric, etc.), this material has got wide applications in various electronic and optoelectronic devices such as in transparent electrodes, solar cell windows, thin film transistor, chemical sensors, etc. (Ref 2–6). ZnO has been exploited in various forms such as single crystal, sintered pellets, thick films, thin films, and hetero-junctions (Ref 7–11). However, thin films are more suitable for the chemical gas sensors because the gas sensing properties are related to

the material surface, where the gases are adsorbed and the chemical reactions occur. More recently, this material has received a growing attention as a nanostructured material because of its excellent properties arising out of large surface-to-volume ratio, quantum confinement effect, etc. (Ref 12–15). As grown ZnO is an n-type semiconductor and its n-type conductivity can be controlled by doping. Various dopants like Al, In, Cu, Sn, etc., have been used to modify the microstructure and defect chemistry of the ZnO matrix. When the doped 3d transition metal (TM) ions have a valence state of 2+, equal to that of Zn, the difference between the ionic radii of Zn and the 3d ions is minimized and thus the defect formation for holding the charge neutrality is suppressed. This has motivated us to investigate the influence of Fe (3d TM) ions on the structural, microstructural, and optical properties of ZnO nanoparticle thin films.

In the present study we have investigated the compositional homogeneity of the Fe-doped ZnO films. Energy dispersive x-ray (EDX) analyses in the scanning electron microscopy (SEM) as well as energy dispersive x-ray spectroscopy mapping have been used to assess the low scale composition and local distribution of elements in the prepared films.

In most of the research work on structural and optical properties of the Fe-doped ZnO thin films, zinc acetate has been used as a host precursor in the film preparation (Ref 16–18). However, very few reports are available on the structural and optical properties of the spray-deposited Fe-doped ZnO thin films using zinc nitrate as a host precursor. So in the present investigation, we have used zinc nitrate as a host precursor in the film preparation.

C.S. Prajapati and P.P. Sahay, Department of Physics, Motilal Nehru National Institute of Technology, Allahabad 211004, India; and Ajay Kushwaha, Department of Physics, Indian Institute of Technology Bombay, Powai, Mumbai 400076, India. Contact e-mail: dr\_ppsahay@rediffmail.com.

**Table 1** Spray process parameters used in the film deposition

Spray parameters	Optimum value/item
Nozzle	Glass
Nozzle-substrate distance	25 cm
Zinc nitrate solution concentration	0.1 M
Solvent	Distilled water
Solution flow rate	~2 mL/min
Carrier gas	Compressed air
Gas pressure	3.2 kg/cm <sup>2</sup>
Substrate temperature	410 ± 10 °C

Baek et al. (Ref 19) and Mishra and Das (Ref 20) have studied the optical properties of the Fe-doped ZnO nanostructures prepared by hydrothermal and co-precipitation method, respectively. Further, ZnCl<sub>2</sub> precursor has been used for synthesis of the Fe-doped films by spray pyrolysis technique by Soumahoro et al. (Ref 21). The gas sensing properties of nanocrystalline Fe-doped ZnO film prepared using spin coating have been investigated by Rambu et al. (Ref 22).

## 2. Experimental Details

The films were deposited on clean glass substrates (microscope slides) by chemical spray pyrolysis technique. The dopant concentration (Fe/Zn at.%) was varied from 0 to 2 at.%. A homogeneous solution was prepared by dissolving requisite amounts of zinc nitrate [0.1 M Zn(NO<sub>3</sub>)<sub>2</sub>·6H<sub>2</sub>O; Merck, India] and ferric chloride [FeCl<sub>3</sub>·6H<sub>2</sub>O; Merck, India] in distilled water at room temperature (300 K). The schematic representation of the spray system of the film deposition has been described elsewhere (Ref 23). The various process parameters used in the film deposition are listed in Table 1. During the course of spray, the substrate temperature was monitored using a chromel-alumel thermocouple with the help of a Motwane digital multimeter (Model: 454). Prior to further investigation, the deposited films were annealed at 500 °C for 1 h. For phase identification and crystallite size determination, the films were examined using a Bruker AXS C-8 advanced diffractometer with CuK $\alpha$  radiation ( $\lambda = 1.5406 \text{ \AA}$ ) as the x-ray source. The surface morphology of the films was investigated with JEOL SEM and EDX analyses with elemental mapping, operated at 15 kV, and NTEGRA atomic force microscopy (AFM). High resolution x-ray photoelectron spectroscopy (XPS) was carried for the chemical composition and electronic structure analyses of the Fe-doped ZnO films. The optical studies of the films were carried out with the help of Perkin Elmer Lambda 35 UV-Vis spectrometer (UK) in the spectral range 350-700 nm. Photoluminescence spectra were done using VARIAN CARY eclipse fluorescence spectrophotometer. The excitation source was a Xenon-lamp (290 nm), and the sample temperature was kept at room temperature. Keithley 2602 dual channel current voltage source meter has been utilized to measure

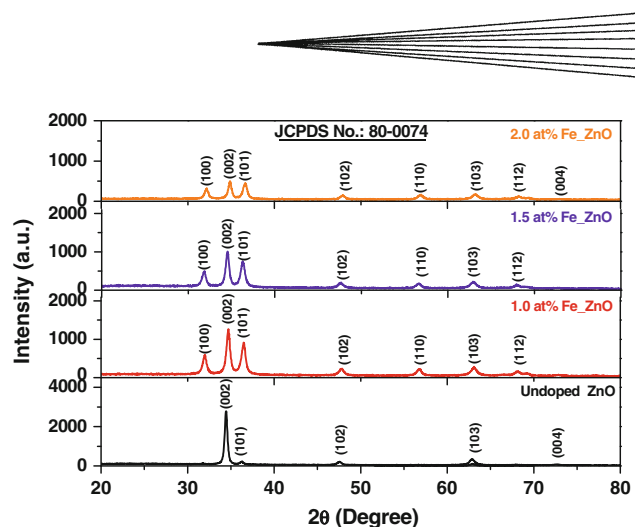


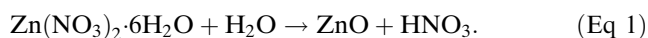
**Fig. 1** XRD spectra of the undoped and Fe-doped ZnO thin films

the photoconductivity properties. A UV lamp with 365 nm centered wavelength and 10 mW total power has been used to excite the sample for photocurrent measurement.

## 3. Results and Discussion

### 3.1 ZnO Film Formation

When aerosol droplets of required solution arrive close to the hot substrates, endothermic decomposition of the fine droplets takes place at the substrate surface, resulting in the formation of ZnO thin films. The substrate temperature and solution flow rate play an important role in the film formation. Possible reaction mechanisms in ZnO film formation are as follow (Ref 23):



The films thus prepared have been found to be well adherent with the glass substrate and almost transparent in physical appearance and were subjected to further analysis.

### 3.2 Structural and Microstructural Analyses

The x-ray diffraction (XRD) spectra of the undoped and Fe-doped ZnO thin films is shown in Fig. 1. The observed diffraction peaks have been found to match with the standard JCPDS file of ZnO, 80-0074, which indicates the formation of wurtzite phase in all the samples. It has been observed that the intensity of the (002) peak decreases and the full width at half maximum (FWHM) increases with increasing Fe-doping concentration, revealing that the crystallinity of the Fe-doped films deteriorates. Similar observations have been found by other researchers (Ref 24, 25). Apart from the intensity and broadness (FWHM) change, the (002) peak position has been found to shift toward the higher angle side. This shift in peak position may be attributed to the replacement of Zn<sup>2+</sup>

Table 2 X-ray diffraction analyses of the undoped and Fe-doped ZnO thin films

ZnO film	Positions, °2 $\theta$	$d$ -Spacing, observed, Å	$d$ -Spacing, (JCPDS), Å	$hkl$	TC	Crystallite size, nm	Average crystallite size, nm	AFM analyses			
								$a = b$ , Å	$c$ , Å	Average grain size, nm	Average surface roughness, nm
0.0 at.% Fe	34.3984	2.6051	2.6075	002	3.8762	40.53	24.39	3.245	5.210	31	6.26
	36.2899	2.4735	2.4789	101	0.0738	26.19					
	47.5145	1.9121	1.9137	102	0.4042	19.03					
	62.9317	1.4757	1.4794	103	0.5212	22.69					
	72.5731	1.3016	1.3037	004	0.1246	13.51					
	31.7642	2.8148	2.8176	100	0.9048	25.88	17.09	3.250	5.182	30	4.46
	34.5883	2.5912	2.6075	002	2.7528	16.59					
	36.2952	2.4731	2.4789	101	0.8617	18.33					
	47.5698	1.9100	1.9137	102	0.7318	15.87					
	56.6148	1.6244	1.6267	110	0.4837	14.13					
	62.9482	1.4754	1.4794	103	0.8134	11.34					
	67.9368	1.3787	1.3801	112	0.4518	17.51					
1.5 at.% Fe	32.1060	2.7856	2.8176	100	0.8636	18.13	17.40	3.217	5.138	29	3.23
	34.8938	2.5692	2.6075	002	2.1114	30.44					
	36.5863	2.4541	2.4789	101	0.7798	15.29					
	47.8555	1.8992	1.9137	102	0.9603	13.61					
	56.8916	1.6172	1.6267	110	0.6751	14.15					
	63.1528	1.4711	1.4794	103	0.9920	17.04					
	68.1406	1.3750	1.3801	112	0.6178	13.14					
	31.9988	2.7947	2.8176	100	0.9424	22.65	17.60	3.227	5.165	24	1.92
	34.7098	2.5824	2.6075	002	3.2395	22.82					
	36.4876	2.4605	2.4789	101	0.9352	20.38					
	47.7787	1.9021	1.9137	102	0.8333	15.88					
	56.8382	1.6186	1.6267	110	0.5636	16.51					
63.0667	1.4729	1.4794	103	0.8713	20.44						
68.0740	1.3762	1.3801	112	0.4815	13.14						
72.8315	1.2976	1.3037	004	0.1333	9.02						

[0.74 Å] ions by Fe<sup>3+</sup> [0.64 Å] ions (Ref 26). As a result, a decrease in lattice parameters “a” and “c” is observed. Similar results have been reported by other workers (Ref 16, 25, 27). On the other hand, Oh et al. (Ref 28), Panigrahy et al. (Ref 29), and Chen et al. (Ref 30) have found that the peak position of (002) gradually shifts toward the smaller angle on increasing the Fe-doping amount. This contradiction in the already published results may be due to existence of different ionic radii of Fe ions (because of different valence states) in a ZnO host matrix. The valence state of Fe ion can be present in Fe<sup>2+</sup> or Fe<sup>3+</sup> or both. The presence of Fe<sup>2+</sup> valence state in the Fe-doped ZnO thin films grown by magnetron sputtering has been confirmed by XPS analysis by Wang et al. (Ref 24), Kim and Park (Ref 26), and Chen et al. (Ref 31). The presence of Fe<sup>3+</sup> ions in the ZnO nanostructure has been suggested by Baek et al. (Ref 19) in the result of XPS analysis of the Fe-doped ZnO nanorods. From these results mentioned above, it may be concluded that the existence of different valence states of Fe ions depends on synthesis technique as well as the precursors used for synthesis. In the present investigation, the diffraction peak shifts toward the higher angle direction with the addition of Fe ions. This implies that atoms of smaller ionic radii are substituted by replacing the host atoms, according to Vegard's law (Ref 32). Thus, shifting toward higher diffraction angle side (shown in Table 1) suggests that in the present investigation the valence state of Fe ions is Fe<sup>3+</sup> in the ZnO film structure.

In order to study the preferential orientation of the films, the texture coefficient (TC) along different peak directions has been calculated. It has been found that the undoped film has best texture along the (002) direction. The crystalline nature of the Fe-doped ZnO films declines on increasing the Fe dopant concentration. The average crystallite size of the doped films has been found to decrease as compared to that of the undoped film. The TC, crystallite size, and lattice parameters have been determined using the required formulae (Ref 23) and are listed in Table 2.

The SEM micrograph of the undoped ZnO thin film is shown in Fig. 2 while the SEM micrographs of the Fe-doped films with elemental mapping are shown in Fig. 3[i(a-d), ii(a-d), iii(a-d)]. The films show good uniformity and dense surface having spherical-shaped grains without visible holes or faulty zones on the film surface. To determine the film thickness, the cross-sectional SEM view of the film (shown in inset of Fig. 2) was taken. The average thickness of all the films was found to be in the range of 800-850 nm.

EDX analyses of the Fe-doped films show that the Fe dopants are incorporated into the ZnO film matrix, and no other elements are present in the system, as shown in Fig. 4(a) to (c). It can be noted that on increasing Fe dopant concentration, the O/Zn ratio in the film moves toward unity (1), implying that ZnO system shifts from non-stoichiometry to stoichiometry. Elemental mapping of the Fe-doped films, shown in Fig. 3[i(a-d), ii(a-d), iii(a-d)], confirm that the films have homogeneous distribution of Zn, O, and Fe for all concentration of Fe dopants. This also

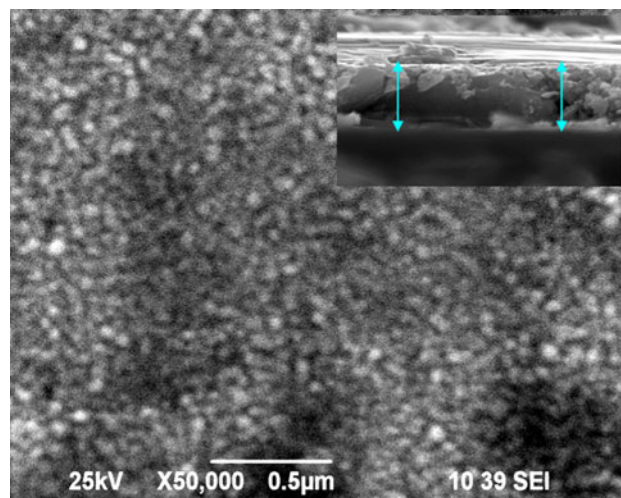


**Fig. 2** SEM micrograph of the undoped ZnO film (inset shows cross-sectional view)

leads to the conclusion that Fe dopants are effectively incorporated into the ZnO film matrix.

The XPS spectra of the 1 at.% Fe-doped ZnO film are shown in Fig. 5(a) to (c). The Fig. 5(a) shows the Zn2p peaks located at 1022.28 and 1045.4 eV, suggesting that the chemical valence state of Zn is 2+ (Ref 33). In Fig. 5(b), the peaks of O1s are found at 530.8 and 532.07 eV which correspond to the lattice oxygen and the adsorbed oxygen on the film surface, respectively (Ref 34). As shown in Fig. 5(c), the peaks located at 711.3 and 718.4 eV correspond to the binding energies of Fe2P<sub>3/2</sub> and Fe2P<sub>3/2</sub>, sat., respectively (Ref 33, 35) whereas the peak at 724.1 eV corresponds to the binding energy of Fe 2P<sub>1/2</sub> (Ref 36), suggesting that the added Fe in the films are in the form of Fe<sup>3+</sup>.

Figures 6(a) to (d) and 7(a) to (d) present the two dimensional (2D) and three dimensional (3D) AFM images of the films as deposited on the glass substrate. The surface morphology of the films reveals that the grains have columnar shapes, which grow preferentially along the c-axis orientation perpendicular to the substrate surface. This film growth may be due to increased lattice strain in the film network, which occurs at the time of film deposition. It may also be due to increased density of nucleation centers with the increasing Fe-doping amount (Ref 37), which in turn, reduces the crystallite size as confirmed by XRD analysis. Similar results have been reported by Xu and Li (Ref 16) and Chen et al. (Ref 30). The average surface roughness and the grain size of the films as function of Fe-doping concentration are listed in Table 2. The average surface roughness and the grain size of the films decrease with the increase of doping concentration, which is in agreement with those reported by Wang et al. (Ref 24) and Bhuvana et al. (Ref 38). Here, Fe dopants act as activators to increase the density of the nucleation centers in the case of doped films, and the film surface becomes more compact as well as smooth with doping.

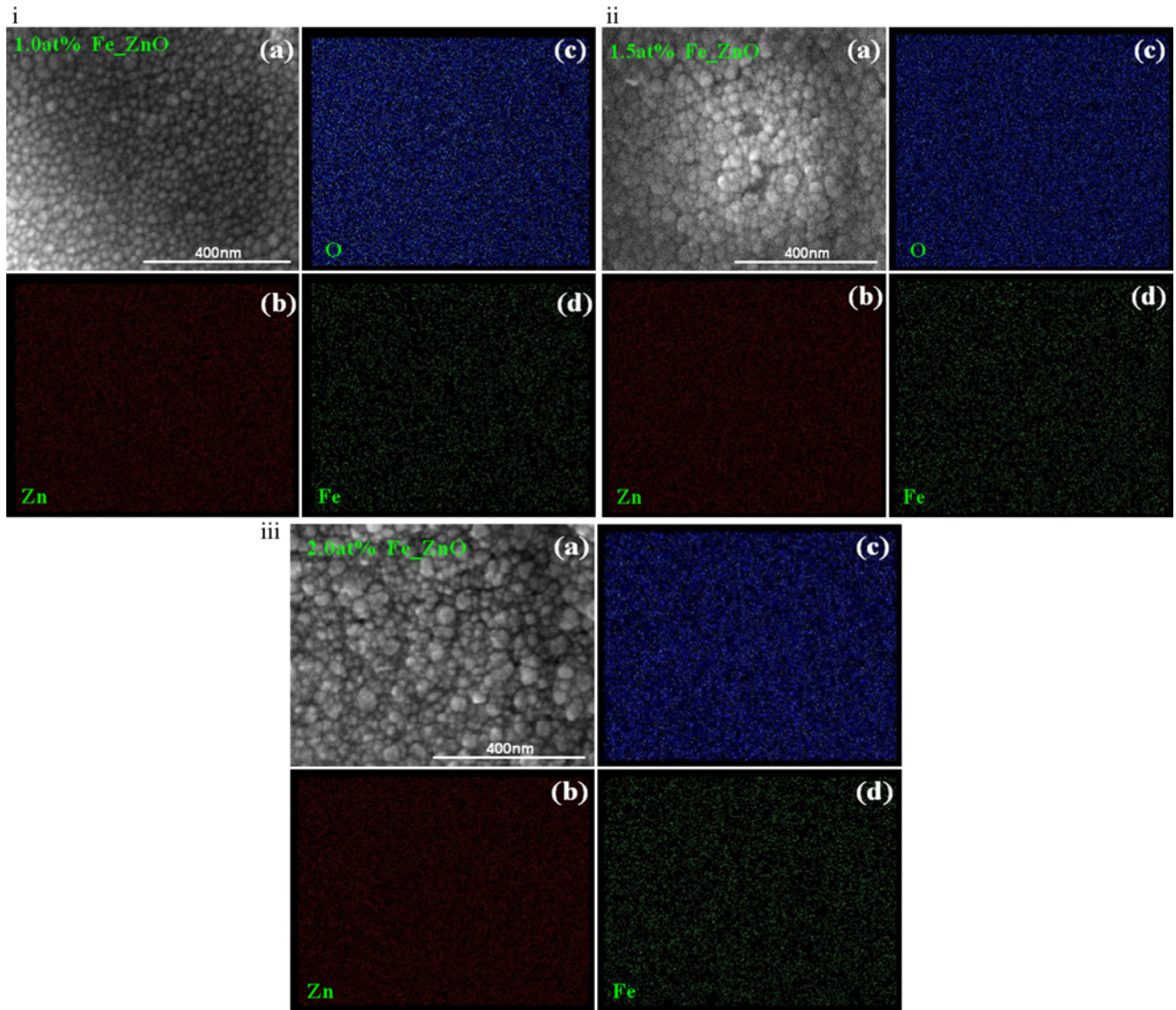


**Fig. 3** [i(a-d), ii(a-d), iii(a-d)]: SEM micrographs of the Fe-doped films with elemental mapping

### 3.3 Optical Properties

Figure 8 shows the optical transmission and absorption spectra of the undoped and Fe-doped films. It has been found that the undoped and 1.0 at.% Fe-doped films show good transparency about 80% while the 1.5 and 2.0 at.% Fe-doped films show transparency approximately 70% in visible region. This continuous decrease in transparency may be due to lattice defects which arise due to Fe ions incorporation into the ZnO host lattice. The decrease in the crystallite size and average surface roughness of the films is also responsible for decreased transmission in the doped films. Similar decrease in transmittance has been observed by Chen et al. (Ref 30) in the study of Fe-doped ZnO thin films prepared by the

radio-frequency magnetron sputtering technique. From Fig. 8, it is also clear that the absorption edge shifts toward the higher wavelength with the increase of Fe doping, suggesting a decrease in the optical band gap. The band gap value,  $E_g$ , has been determined by the extrapolation of the linear part of the  $(Ah\nu)^2$  versus  $h\nu$  variation to  $Ah\nu=0$ . Figure 9 describes the plots of  $(Ah\nu)^2$  as a function of  $h\nu$ . It is noticed that when the Fe content increases from 0 to 2.0 at.%, the band gap value decreases from 3.30 to 3.17 eV. Similar pattern in the band gap decrement has been reported earlier also (Ref 33). This band gap decrease is due to increase in the band tail (Urbach tail) width which is related to the lattice disorder in the film network.

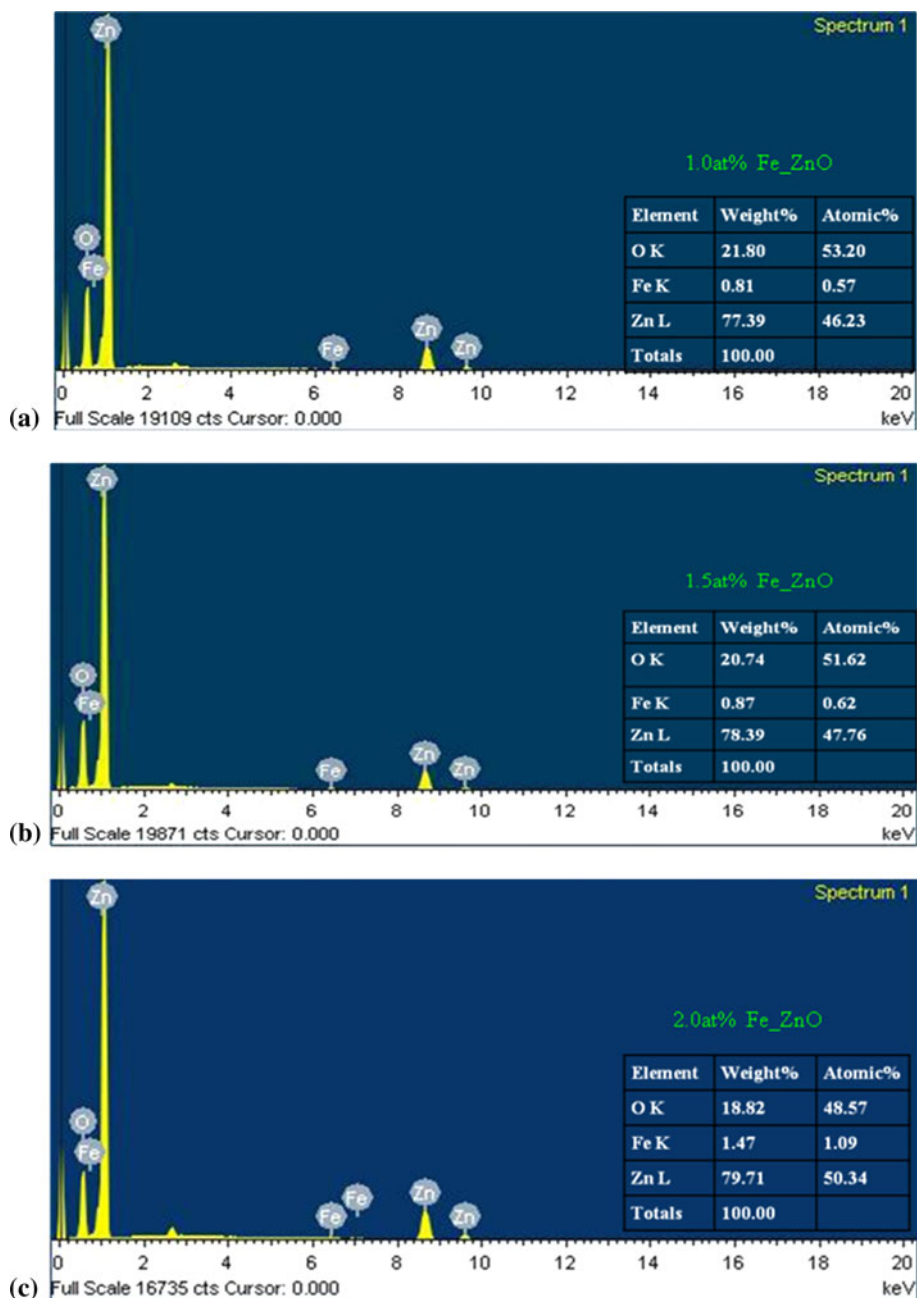


**Fig. 4** (a) to (c) EDX analyses of the Fe-doped ZnO thin films

The absorption coefficient  $\alpha$  near the fundamental absorption edge is found to be exponentially dependent on the incident photon energy and obeys the well-known Urbach relation expressed as (Ref 39):

$$\alpha = \alpha_0 \exp\left(\frac{h\nu}{E_0}\right) \quad (\text{Eq 2})$$

where  $\alpha_0$  is a constant and  $E_0$  is a parameter describing the width of the tail of localized states in the band gap.

In terms of absorption, the Eq 2 can be written as

$$A = A_0 \exp\left(\frac{h\nu}{E_0}\right) \quad (\text{Eq 3})$$

where  $A_0$  is another constant.  $E_0$  is estimated from the slope of the linear relationship  $\ln A$  against  $h\nu$ , shown in Fig. 10. These values of  $E_0$  have been found to be in agreement with the band gap decrement.

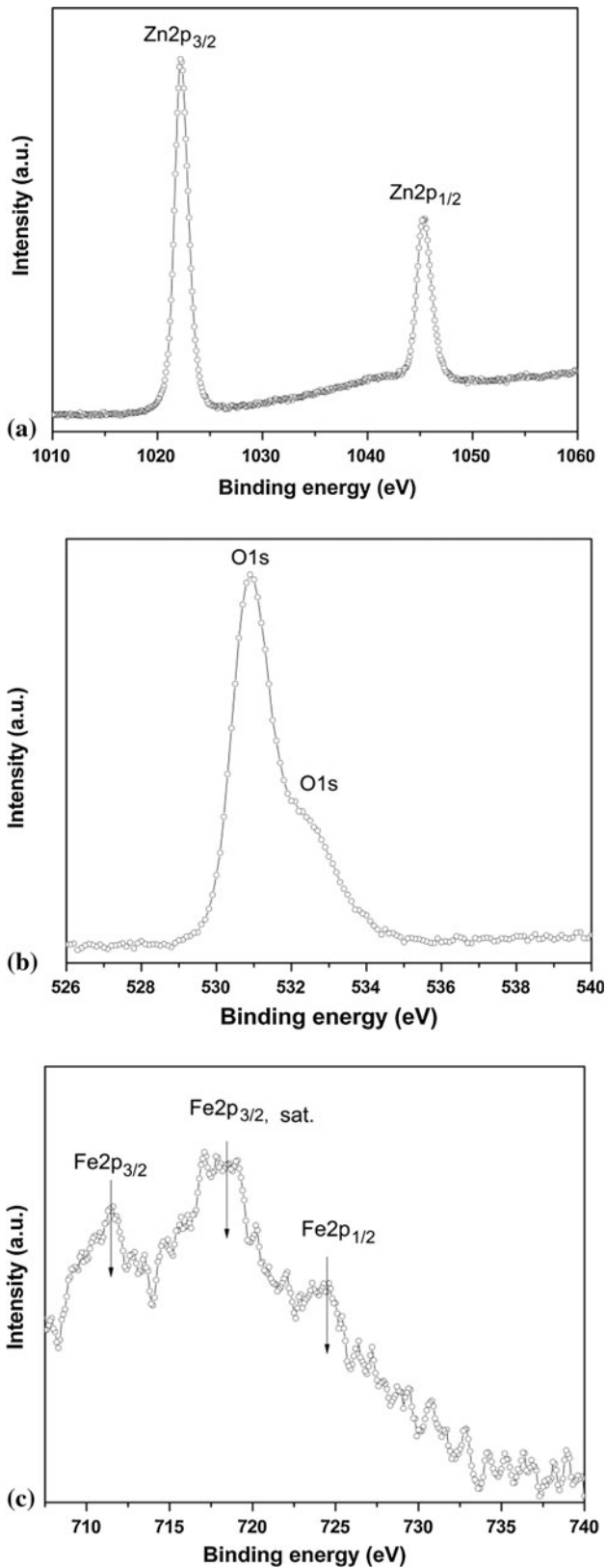


Fig. 5 (a) to (c) XPS spectra of the 1 at.% Fe-doped ZnO film

The refractive index dispersion behavior of the films has also been studied since the dispersion being a significant factor in optical communication devices, plays an important role in the research for optical materials. The refractive index,  $n$ , has been determined from reflectance data using the relation (Ref 40):

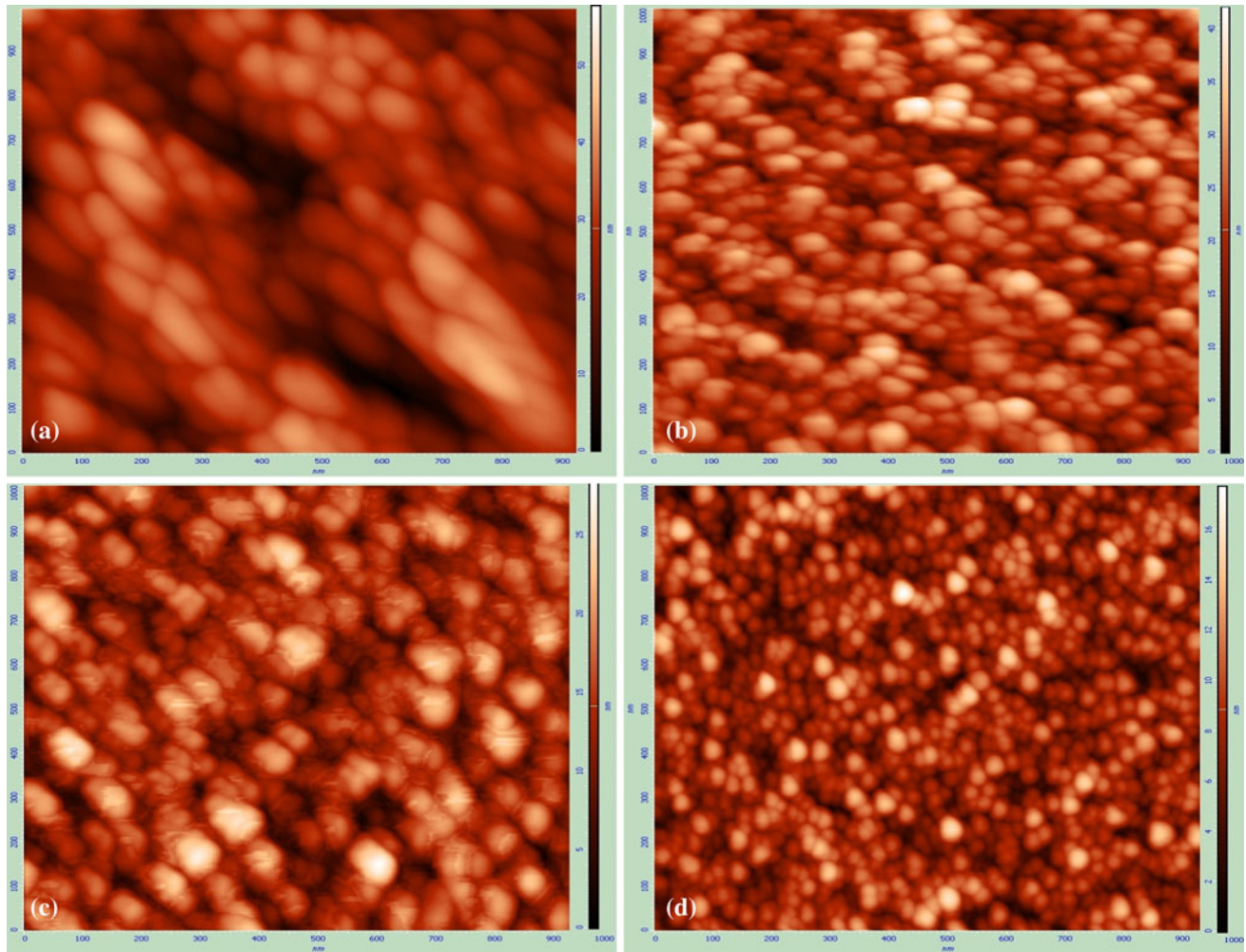
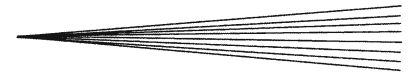
$$R = \frac{(n-1)^2}{(n+1)^2}. \quad (\text{Eq 4})$$

Figure 11 depicts the variation of reflectance spectra of the films with wavelength in the range 350-700 nm. The dispersion of the refractive index is fitted to the Cauchy relation:

$$n = \alpha + \left( \frac{\beta}{\lambda^2} \right) \quad (\text{Eq 5})$$

where  $\alpha$  and  $\beta$  are the Cauchy's constants and  $\lambda$  is the wavelength of the light used. It is observed that the refractive index of the undoped film satisfy the relation  $1.5682 + 0.94 \times 10^5/\lambda^2$  while those of 1.0, 1.5, and 2.0 at.% Fe-doped film satisfies the relation  $1.9519 + 0.97 \times 10^5/\lambda^2$ ,  $2.2505 + 1.06 \times 10^5/\lambda^2$ , and  $2.45 + 0.72 \times 10^5/\lambda^2$ , respectively. Figure 12 indicates that the undoped and 1.5 at.% Fe-doped films have normal dispersion for the wavelength range 550-700 nm while the 1 at.% Fe-doped film has normal dispersion for the wavelength range 450-700 nm. The solid curve in Fig. 12 represents the Cauchy fit. The discrepancy in Cauchy's fit is due to limitations of this relation and it is highly dependent on material properties. The refractive index of the Fe-doped films in the visible region (at 575 nm wavelength) has been determined in the range 2.27-2.68.

Transient photocurrent measurements (shown in Fig. 13) have been carried out to analyze the UV light photosensitivity of the undoped and Fe-doped ZnO thin films. Dark and photo currents measured as a function of applied voltage are shown in Fig. 14(a) and (b). It has been observed that the UV light luminescence increases film conductivity. ZnO films adsorb atmospheric oxygen on the surface by capturing free electrons from the conduction band [ $\text{O}_2(\text{air}) \leftrightarrow \text{O}_2(\text{ads}); \text{O}_2(\text{ads}) + e^- \rightarrow \text{O}_2^-(\text{ads})$ ], which creates a depletion layer near the film surface, resulting in low dark current. Upon exposure to illumination on film surface, electron-hole pairs are generated, which cause increase in photocurrent. During this process, holes recombine with the  $\text{O}_2^-$  trapped electrons and release  $\text{O}_2$  from the surface [ $\text{O}_2^-(\text{ads}) + h^+ \rightarrow \text{O}_2(\text{gas})$ ]. The unpaired electrons in the system contribute gradually to increase the photocurrent during illumination until an equilibrium state is reached (Ref 41), which is governed by desorption and re-adsorption of  $\text{O}_2$  molecules on the film surface. As the light is turned on/off, the slow response and recovery in conductance is observed which may be attributed to the oxygen adsorption and desorption process (Ref 42, 43). The holes density is much less than that of electrons. As a result, upon turning off light, holes combine quickly



**Fig. 6** (a) to (d) 2D AFM images of (a) 0 at.%, (b) 1.0 at.%, (c) 1.5 at.%, and (d) 2.0 at.% Fe-doped ZnO thin films

with the electrons but due to higher density of electrons, still some electrons are left to recombine, resulting in slow decay of current. Films having small grains show higher resistance, resulting in slow increase in photocurrent (Ref 44).

ZnO is one of the good fluorescence materials, which generates emissions such as ultraviolet emission (~380 nm), blue emission (~460 nm), green emission (~540 nm), and red emission (~630 nm) (Ref 45). Doping in ZnO influences the band to band as well as the visible emission spectra to a great extent. Bin et al. (Ref 34) have studied the photoluminescence property of the Fe-doped ZnO nanocantilever arrays synthesized by thermal evaporating method and found the red shift at ~536 nm for the doped film as well as a quenched intensity compared to the undoped film. Effects of Fe doping on the luminescence spectra have also been studied by Inamdar et al. (Ref 27) where it has been reported that the undoped ZnO nanocrystals show

maxima at ~385 nm along with blue and green luminescence, and a red shift is observed from the undoped to the Fe-doped nanocrystals with quenching in emission intensity. Oh et al. (Ref 28) have synthesized ZnO nanorods via a sonochemical route and found enhanced deep level PL intensity on Fe doping. Green-orange emission and near band emission (NBE) has been reported by Panigrahy et al. (Ref 29) in the study of Fe-doped ZnO nanorods synthesized by low temperature method. These results indicate that luminescence in ZnO nanostructures depends on fabrication conditions of the sample and also the method used in the growth process.

In the present investigation, to study the influence of Fe doping on the luminescence of the ZnO films, the PL spectra (shown in Fig. 15) of the ZnO films with different Fe-doping concentration at room temperature were taken, under the excitation of 290 nm Xe-lamp light source. The ultraviolet emission centered at ~390 nm for the undoped



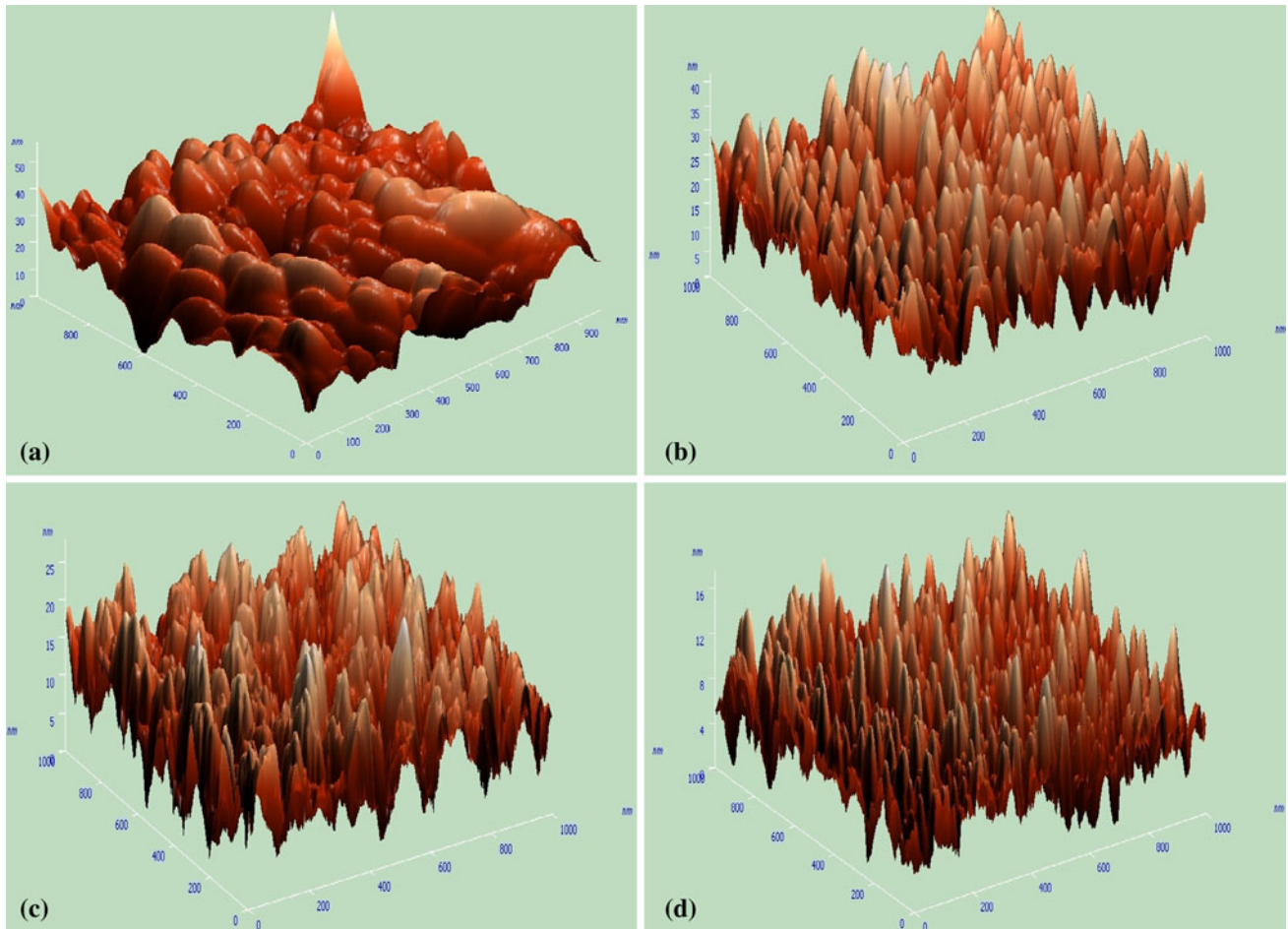


**Fig. 7** (a) to (d) 3D AFM images of (a) 0 at.%, (b) 1.0 at.%, (c) 1.5 at.%, and (d) 2.0 at.% Fe-doped ZnO thin films

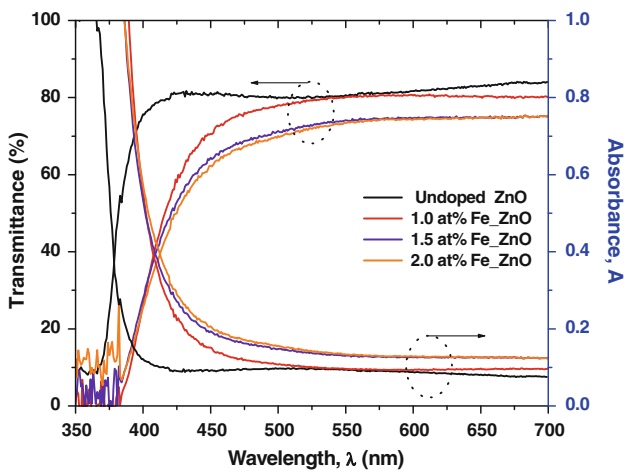


**Fig. 8** Optical transmittance and absorbance spectra of the undoped and Fe-doped ZnO thin films

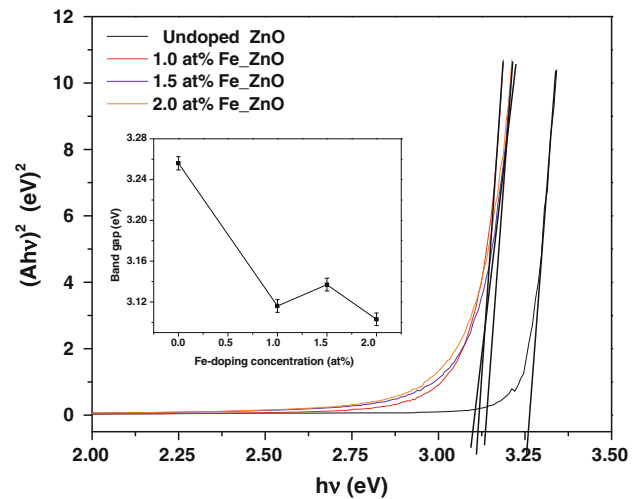


**Fig. 9** Plots of  $(Ahv)^2$  vs  $h\nu$

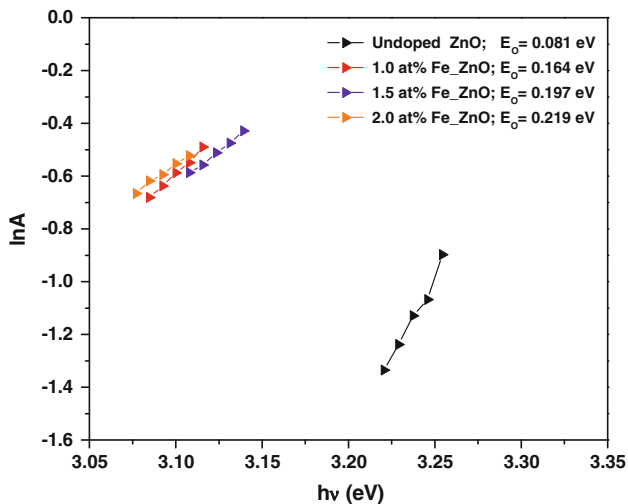


Fig. 10  $\ln A$  vs  $h\nu$  plot

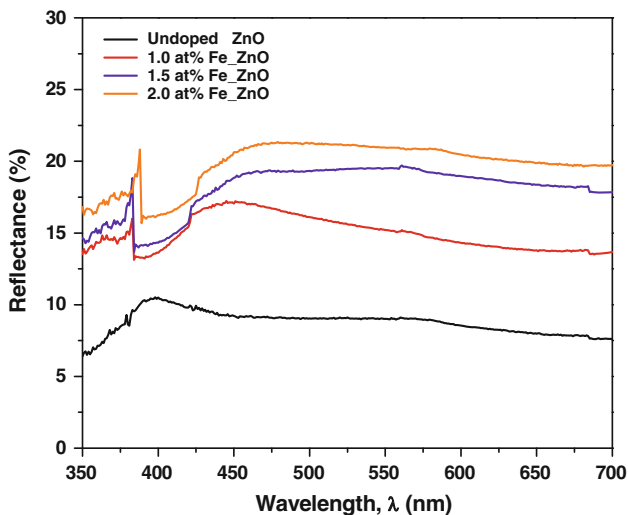


Fig. 11 Reflectance spectra of the undoped and Fe-doped ZnO films

film is observed in the spectra. Generally, ZnO shows PL emission in two parts: the NBE (near band edge) spectra and DL (deep level) emission spectra (Ref 46). But in the present investigation, only the NBE spectra have been observed in all the films, which arise due to free exciton recombination through an exciton-exciton collision process (Ref 47). With the increase of Fe-doping concentration up to 1 at.%, an enhancement in the intensity of ultraviolet emission centered at  $\sim 388$  nm has been observed, and on further doping, the intensity reduces. Similar variation in intensity has been observed by Xu and Li (Ref 16) in the study of 1 at.% Fe-doped ZnO thin films prepared by sol-gel technique, where it has been reported

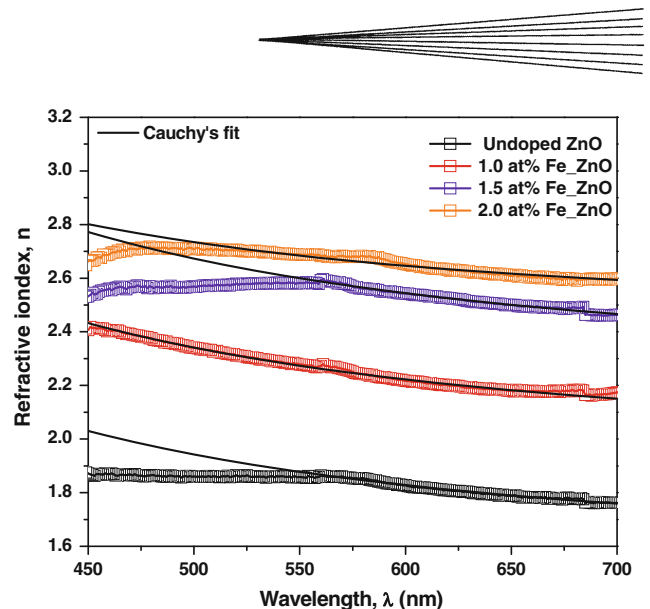


Fig. 12 Variation of refractive index and Cauchy's fit as a function of wavelength

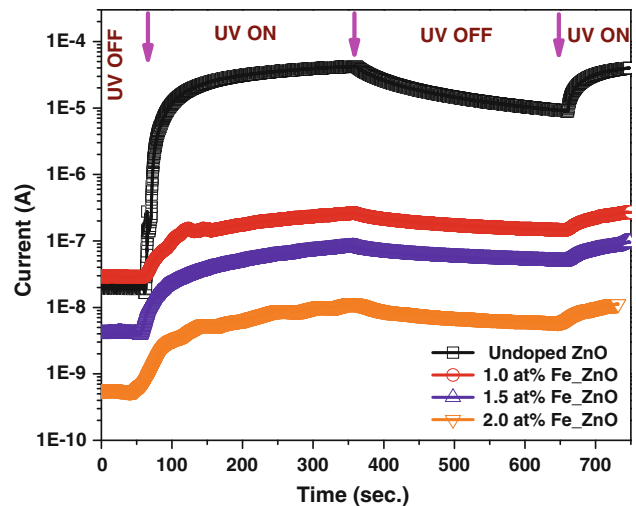


Fig. 13 Photocurrent growth and decay curves of the undoped and Fe-doped films

that emission intensity of peak centered at 381 nm reduces due to decline in the crystal quality of 3 and 5 at.% Fe-doped ZnO films, as the poor crystal quality reduces the free exciton density. A small blue shift in the PL spectra has been observed on Fe doping (inset of Fig. 15). This blue shift may be attributed to the substitution of  $\text{Fe}^{3+}$  ions in place of  $\text{Zn}^{2+}$  ions in ZnO host lattice, leading to lattice disorder resulting in band structure deformation. Similar blue shift in PL spectra has been observed by Mishra and Das (Ref 20). Wang et al. (Ref 48) have reported the significant blue shift for the higher Fe-doping concentration in the study of ZnO nanocrystals obtained by thermolysis method.

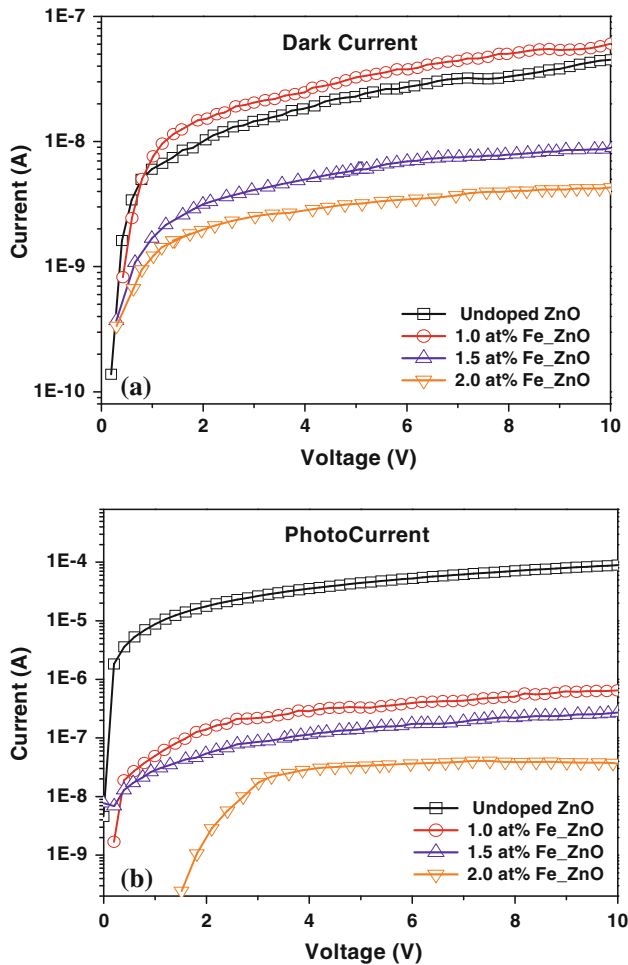


Fig. 14 (a) Dark and (b) photo currents with applied voltage

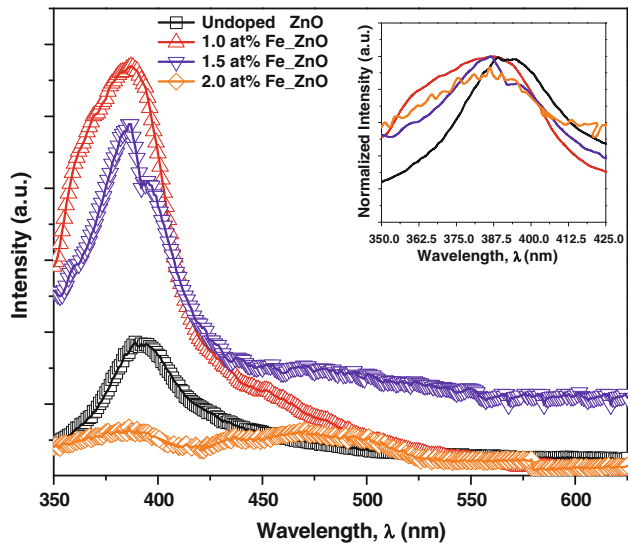


Fig. 15 Photoluminescence spectra of the undoped and Fe-doped ZnO films (inset shows PL normalized intensity plots)

## 4. Conclusion

All the spray-deposited ZnO thin films are found to be in hexagonal wurtzite structure. Fe-doping incorporation into ZnO lattice has been confirmed by XRD measurements. The SEM images of the undoped and Fe-doped ZnO films reveal that the films have spherical-shaped grains with continuous smooth surface. EDX analyses of the Fe-doped films show that the Fe dopants are incorporated into the ZnO film matrix. High resolution XPS studies confirm the presence of 3+ oxidation state of Fe in the doped films. AFM images show that the average surface roughness of the films decreases from the undoped to the doped films.

After Fe doping, due to reduction in the surface roughness, the optical reflectance of the films has been found to increase. The optical absorption edge shifts toward the higher wavelength and the band gap value decreases from 3.30 to 3.17 eV on Fe doping. The films have been found to be photosensitive. Dark current has been found to increase from the undoped to the 1 at.% Fe-doped film. Photoluminescence spectra of the Fe-doped films reveal that the 1 at.% Fe-doped film shows a strong ultraviolet emission centered at  $\sim 388$  nm.

## Acknowledgments

The authors are thankful to the Head, Indian Instrument Center of Indian Institute of Technology, Roorkee, India for providing facilities for XRD and AFM characterization. They are also thankful to Prof. M. Aslam, Department of Physics, for providing SEM facility and Prof. D. Bahadur, Department of Metallurgical Engineering and Materials Science, Indian Institute of Technology Bombay, India for photoconductivity as well as PL measurement facilities. The financial support provided by the Department of Science & Technology, Govt. of India, in the form of a research project (No. SR/S2/CMP-41/2008) is gratefully acknowledged.

## References

1. Z.L. Wang, Zinc Oxide Nanostructures: Growth, Properties and Applications, *J. Phys.: Condens. Mater.*, 2004, **16**, p R829-R858
2. M. Suche, S. Christoulakis, K. Moschovis, N. Katsarakis, and G. Kiriakidis, ZnO Transparent Thin Films for Gas Sensor Applications, *Thin Solid films*, 2006, **515**, p 551-554
3. P. Mitra, A.P. Chatterjee, and H.S. Maiti, ZnO Thin Film Sensor, *Mater. Lett.*, 1998, **35**, p 33-38
4. B. Bhooloka Rao, Zinc Oxide Ceramic Semi-Conductor Gas Sensor for Ethanol Vapour, *Mater. Chem. Phys.*, 2000, **64**, p 62-65
5. N. Koshizaki and T. Oyama, Sensing Characteristics of ZnO-Based NO<sub>x</sub> Sensor, *Sens. Actuators B*, 2000, **66**, p 119-121
6. K. Arshak and I. Gaiden, Development of a Novel Gas Sensor Based on Oxide Thick Films, *Mater. Sci. Eng. B*, 2005, **118**, p 44-49
7. A. Jones, T.A. Jones, B. Mann, and J.G. Firth, The Effect of the Physical form of the Oxide on the Conductivity Changes Produced by CH<sub>4</sub>, CO and H<sub>2</sub>O on ZnO, *Sens. Actuators B*, 1984, **5**, p 75-88



8. S. Saito, M. Miyayama, K. Kounoto, and H. Yanagida, Gas Sensing Characteristics of Porous ZnO and Pt/ZnO Ceramics, *J. Am. Ceram. Soc.*, 1985, **68**, p 40-43
9. S. Pizzini, N. Buttá, D. Narducci, and M. Palladino, Thick Film ZnO Resistive Gas Sensors, *J. Electrochem. Soc.*, 1989, **136**, p 1945
10. S. Roy and S. Basu, Improved Zinc Oxide Film for Gas Sensor Applications, *Bull. Mater. Sci.*, 2002, **25**, p 513-515
11. S. Basu and A. Dutta, Modified Heterojunction Based on Zinc Oxide Thin Film for Hydrogen Gas-Sensor Application, *Sens. Actuators B*, 1994, **22**, p 83-87
12. X.L. Cheng, H. Zhao, L.H. Huo, S. Gao, and J.G. Zhao, ZnO Nanoparticulate Thin Film: Preparation, Characterization and Gas-Sensing Property, *Sens. Actuators B*, 2004, **102**, p 248-252
13. O. Lupan, V.V. Ursaki, G. Chai, L. Chow, G.A. Emelchenko, I.M. Tiginyanu, A.N. Gruzintsev, and A.N. Redkin, Selective Hydrogen Gas Nanosensor Using Individual ZnO Nanowire with Fast Response at Room Temperature, *Sens. Actuators B*, 2010, **144**, p 56-66
14. O. Lupan, G. Chai, and L. Chow, Novel Hydrogen Gas Sensor Based on Single ZnO Nanorods, *Microelectron. Eng.*, 2008, **85**, p 2220-2225
15. C.S. Prajapati, S.N. Pandey, and P.P. Sahay, Sensing of LPG with Nanostructured Zinc Oxide Thin Films Grown by Spray Pyrolysis Technique, *Phys. B*, 2011, **406**, p 2684-2688
16. L. Xu and X. Li, Influence of Fe-Doping on the Structural and Optical Properties of ZnO Thin Films Prepared by Sol-Gel Method, *J. Cryst. Growth*, 2010, **312**, p 851-885
17. M. Sahal, B. Hartiti, A. Ridah, M. Mollar, and B. Mari, Structural, Electrical and Optical Properties of ZnO Thin Films Deposited by Sol-Gel Method, *Microelectron. J.*, 2008, **39**, p 1425-1428
18. H.H. Hsu, H. Paul Wang, C.Y. Chen, C.J.G. Jou, and Y.-L. Wei, Chemical Structure of Zinc in the Fe/ZnO Thin Films During Sensing of Ethanol, *J. Electron. Spectrosc. Relat. Phenom.*, 2007, **156-158**, p 344-346
19. S. Baek, J. Song, and S. Lim, Improvement of the Optical Properties of ZnO Nanorods by Fe Doping, *Phys. B*, 2007, **399**, p 101-104
20. A.K. Mishra and D. Das, Investigation on Fe-Doped ZnO Nanostructures Prepared by a Chemical Route, *Mater. Sci. Eng. B*, 2010, **171**, p 5-10
21. I. Soumahoro, R. Moubah, G. Schmerber, S. Colis, M. Ait Aouaj, M. Abd-lefdil, N. Hassanain, A. Berrada, and A. Dinia, Structural, Optical, and Magnetic Properties of Fe-Doped ZnO Films Prepared by Spray Pyrolysis Method, *Thin Solid Films*, 2010, **518**, p 4593-4596
22. A.P. Rambu, C. Doroftei, L. Ursu, and F. Iacomi, Structure and Gas Sensing Properties of Nanocrystalline Fe-Doped ZnO Films Prepared by Spin Coating Method, *J. Mater. Sci.*, 2013, **48**, p 4305-4312
23. C.S. Prajapati and P.P. Sahay, Growth, Structure and Optical Characterization of Al-Doped ZnO Nanoparticle Thin Films, *Cryst. Res. Technol.*, 2011, **46**, p 1086-1092
24. C. Wang, Z. Chen, Y. He, L. Li, and D. Zhang, Structure, Morphology and Properties of Fe-Doped ZnO Films Prepared by Facing-Target Magnetron Sputtering System, *Appl. Surf. Sci.*, 2009, **255**, p 6881-6887
25. W.-G. Zhang, B. Lu, L.-Q. Zhang, J.-G. Lu, M. Fang, and K.-W. Wu, Influence of Preparation Condition and Doping Concentration of Fe-Doped ZnO Thin Films: Oxygen-Vacancy Related Room Temperature Ferromagnetism, *Thin Solid Films*, 2011, **519**, p 6624-6628
26. K.J. Kim and Y.R. Park, Optical Investigation of  $Zn_{1-x}Fe_xO$  Films Grown on  $Al_2O_3(0001)$  by Radio-Frequency Sputtering, *J. Appl. Phys.*, 2004, **96**, p 4150-4153
27. D.Y. Inamdar, A.K. Pathak, I. Dubenko, N. Ali, and S. Mahamuni, Room Temperature Ferromagnetism and Photoluminescence of Fe Doped ZnO Nanocrystals, *J. Phys. Chem. C*, 2011, **115**, p 23671-23676
28. E. Oh, S.H. Jung, S. Yu, and S.J. Rhee, Vertically Aligned Fe-Doped ZnO Nanorod Arrays by Ultrasonic Irradiation and Their Photoluminescence Properties, *Mater. Lett.*, 2008, **62**, p 3456-3458
29. B. Panigrahy, M. Aslam, and D. Bahadur, Effect of Fe Doping Concentration on Optical and Magnetic Properties of ZnO Nanorods, *Nanotechnology*, 2012, **23**, p 115601-115606
30. Z.C. Chen, L.J. Zhunge, X.M. Wu, and Y.D. Meng, Initial Study on the Structure and Optical Properties of  $Zn_{1-x}Fe_xO$  Films, *Thin Solid Films*, 2007, **515**, p 5462-5465
31. A.J. Chen, X.M. Wu, Z.D. Sha, L.J. Zhunge, and Y.D. Meng, Structure and Photoluminescence Properties of Fe-Doped ZnO Thin Films, *J. Phys. D: Appl. Phys.*, 2006, **39**, p 4762-4765
32. A.R. Denton and N.W. Ashcroft, Vegard's law, *Phys. Rev. A: At. Mol. Opt. Phys.*, 1991, **43**, p 3161-3164
33. X.C. Wang, W.B. Mi, and D.F. Kuang, Microstructure, Magnetic and Optical Properties of Sputtered Polycrystalline ZnO Films with Fe Addition, *Appl. Surf. Sci.*, 2010, **256**, p 1930-1935
34. B. Zhang, S. Zhou, H. Wang, and Z. Du, Raman Scattering and Photoluminescence of Fe-Doped ZnO Nanocantilever Arrays, *Chin. Sci. Bull.*, 2008, **53**, p 1639-1643
35. M. Mullet, V. Khare, and C. Ruby, XPS Study of Fe(II)-Fe(III) (oxy) Hydroxycarbonate Green Rust Compounds, *Surf. Interface Anal.*, 2008, **40**, p 323-328
36. B.V. Appa Rao, S. Srinivasa Rao, and M. Sarath Babu, Synergistic Effect of NTMP,  $Zn^{2+}$  and Ascorbate in Corrosion Inhibition of Carbon Steel, *Ind. J. Chem. Technol.*, 2005, **12**, p 629-634
37. F. Paraguay, D.J. Morales, W. Estrada, L.E. Andrade, and M. Miki-Yoshida, Influence of Al, In, Cu, Fe and Sn Dopants in the Microstructure of Zinc Oxide Thin Films Obtained by Spray Pyrolysis, *Thin Solid Films*, 2000, **366**, p 16-27
38. K.P. Bhuvana, J. Elanchezhyan, N. Gopalakrishnan, and T. Balasubramanian, Codoped (AlN) and Monodoped (Al) ZnO Thin Films Grown by RF Sputtering: A Comparative Study, *Appl. Surf. Sci.*, 2008, **255**, p 2026-2029
39. F. Urbach, The Long-Wavelength Edge of Photographic Sensitivity and of the Electronic Absorption of Solids, *Phys. Rev.*, 1953, **92**, p 1324
40. A. Goswami, *Thin Film Fundamentals*, New Age International, New Delhi, 1996
41. X.G. Zheng, Q.Sh. Li, W. Hu, D. Chen, N. Zhang, M.J. Shi, J.J. Wang, and L.Ch. Wang, Photoconductive Properties of ZnO Thin Films Grown by Pulsed Laser Deposition, *J. Lumin.*, 2007, **122-123**, p 198-201
42. H. Kind, H. Yan, B. Messer, M. Law, and P. Yang, Nanowire Ultraviolet Photodetectors and Optical Switches, *Adv. Mater.*, 2002, **14**, p 158-160
43. S. Kumar, V. Gupta, and K. Sreenivas, Synthesis of Photoconducting ZnO Nano-Needles Using an Unbalanced Magnetron Sputtered ZnO/Zn/ZnO Multilayer Structure, *Nanotechnology*, 2005, **16**, p 1167-1171
44. R. Ayouchi, L. Bentes, C. casteleiro, O. Conde, C.P. Marques, E. Alves, A.M.C. Moutinho, H.P. Marques, O. Teodoro, and R. Schwarz, Photosensitivity of Nanocrystalline ZnO Films Grown by PLD, *Appl. Surf. Sci.*, 2009, **255**, p 5917-5921
45. A. Ghosh, N.G. Deshpande, Y.G. Gudage, R.A. Joshi, A.A. Sagade, D.M. Phase, and R. Sharma, Effect of Annealing on Structural and Optical Properties of Zinc Oxide Thin Film Deposited by Successive Ionic Layer Adsorption and Reaction Technique, *J. Alloys Compds.*, 2009, **469**, p 56-60
46. M. Wang, E.J. Kim, and S.H. Hahn, Photoluminescence Study of Pure and Li-Doped ZnO Thin Films Grown by Sol-Gel Technique, *J. Lumin.*, 2011, **131**, p 1428-1433
47. W. Shan, W. Walukiewicz, J.W. Ager, K.M. Yu, H. Yuan, H.P. Xin, G. Cantwell, and J.J. Song, Nature of Room-Temperature Photoluminescence in ZnO, *Appl. Phys. Lett.*, 2005, **86**, p 191911-191913
48. Y.S. Wang, P.J. Thomas, and P.O. Brien, Optical Properties of ZnO Nanocrystals Doped with Cd, Mg, Mn, and Fe Ions, *J. Phys. Chem. B*, 2006, **110**, p 21412-21415